Picosecond carrier dynamics and studies of Auger recombination processes in indium arsenide at room temperature

K. L. Vodopyanov

General Physics Institute, Vavilov Street 38, 117942 Moscow, Russia

H. Graener

EP 111, Universität Bayreuth, Postfach 101251, D-8580 Bayreuth, Federal Republic of Germany

C. C. Phillips

Solid State Group, Physics Department, Imperial College, London SW7 2BZ, United Kingdom

T. J. Tate

Department of Electrical Engineering, Imperial College, London SW7 2AZ, United Kingdom

(Received 20 April 1992)

Pump-probe midinfrared spectroscopic experiments with 10-ps resolution have been performed in ultrathin (0.09–3.3 μm) undoped molecular-beam epitaxy InAs epilayers on GaAs substrates near and above the fundamental absorption edge ($h\nu=0.335-0.485$ eV). Significant bleaching due to a dynamic Moss-Burstein effect was seen near the excitation photon frequency. Bleaching recovery times in the range 3000–35 ps were found, and were strongly dependent on the pump photon energy, InAs epilayer thickness, and irradiation dose in the case of layers implanted with high-energy protons. The measured evolution of the excess carrier distributions as a function of delay after excitation allowed the coefficient for Auger recombination in InAs to be measured as $1.1\pm0.1\times10^{-26}$ cm^6 s^{-1}. The carrier recombination rates were found to be governed by the Auger effect for "thick" (>0.5 μm) samples and by a recombination velocity of $\approx2.7\times10^4$ cm s^{-1} at the dislocated InAs/GaAs heterointerface for "thin" (<0.5 μm) samples.

I. INTRODUCTION

InAs is a direct narrow-gap semiconductor and exhibits large optical nonlinearities near the fundamental absorption edge. A number of nonlinear absorption and refraction properties associated with the fundamental band-gap resonance have been studied previously and have potential for use in such fields as all-optical switching, optical bistability, optical signal processing, four-wave mixing, and laser intracavity control.

Optical bistability was observed in n-type InAs ($n_e=2\times10^{16}$ cm^{-3}, $T=77$ K), with a hydrogen fluoride (HF) laser power of only 3 mW (focused peak intensity 75 W/cm^2).[1] The 3.096-μm HF laser line closely matches the 77-K InAs band gap and the observed nonlinear refraction was ascribed to the creation of conduction-band electrons. Under similar experimental conditions significant absorption saturation was also seen at power levels of 2 mW (intensity 12 W/cm^2),[2] in reasonable agreement with the dynamic Moss-Burstein shift (DMS) model. Three-photon absorption of CO_2 laser radiation has also been used to create absorption and refractive index gratings for four-wave mixing and phase conjugation of 10.6-μm laser radiation.[3]

The room-temperature nonlinear absorption properties of nominally undoped InAs have recently been studied using $\lambda=2.94$-μm ($h\nu=0.412$ eV), 100-ps Er^{3+}:YAG laser pulses (where YAG denotes yttrium aluminum garnet).[4] 3.3-μm-thick InAs single-crystal films grown on transparent GaAs substrates by molecular-beam-epitaxial (MBE) growth were studied. The room-temperature InAs band gap $E_g=0.35$ eV,[5] corresponds to $\lambda=3.54$ μm (2825 cm^{-1}), so that the laser photon energy was 71 meV ($\approx20\%$) above the band gap. Absorption saturation was found at laser energy fluences of less than 10 mJ/cm^2, in good agreement with the DMS model. The measured bleaching recovery times of about 200 ps were mainly determined by nonradiative carrier recombination. This rapid bleaching effect has since been used to achieve passive Q switching and passive mode locking of an Er:YSGG laser ($\lambda=2.79$ μm).[6] In the case of pure Q switching, pulses with 150–200-ns duration and 5-mJ energy were generated. In the case of mode locking, the output was in the form of a train of 20–30 pulses with about a 30-ps pulse duration and a total energy of 5–10 mJ.

The requirements of the lifetime in InAs depend on the nature of its intended application. Low-threshold nonlinear optical devices controlled by cw lasers and high-sensitivity midinfrared detectors and emitters need large excess carrier lifetimes, whereas applications such as laser mode locking, ultrafast radiation detectors, and optical switches require recovery times as short as possible.

II. EXPERIMENTAL SETUP

Undoped 0.09–3.3-μm-thick InAs epilayers were grown by low-temperature MBE on GaAs substrates.[7] The as-grown wafers all had measured 77-K Hall carrier

concentrations of $n \approx 5 \times 10^{14}$ cm^{-3} and were intrinsic ($n_i \approx 8.25 \times 10^{14}$ cm^{-3}) at room temperature. Low-temperature (10-K) small-signal optical-absorption spectra[8] showed pronounced excitonic structure at the band edge and a complete absence of Urbach tail states, evidencing the excellent single-crystal quality of the InAs epilayers.

A double-resonance IR ps spectrometer based on LiNbO$_3$ parametric superradiant generators pumped by a Nd:YAG laser[9] was used for the pump-probe studies. The pump and probe pulses had a duration of 12 ps and were independently tunable in the range 2700–3900 cm^{-1} (0.335–0.485 eV) at a repetition rate of 1–2 Hz.

In order to avoid interference effects and surface reflection losses, all pump-probe measurements were performed at the InAs Brewster angle of 74°. The pump pulse (with an energy of 20–40 mJ) was focused onto the sample (Fig. 1), using a 50-cm focal length CaF$_2$ lens, to give an elliptical spot area of 16.3 mm.^{2} The probe pulse had an energy three orders of magnitude smaller and a spot area of 0.25 mm^2 (Fig. 2). The angle between the pump and probe beams was 13.5° and their polarizations were in the plane of incidence.

The pump photons with energy higher than the InAs band gap create a nonequilibrium excess electron and hole population, which then causes a dynamic blueshift in the ir absorption edge due to band filling as the pump radiation is absorbed. Net absorption of the pump radiation ceases when the sum of the electron and hole Fermi occupation factors of the conduction- and valence-band states linked by the photon field $f_e + f_h$ closely approaches unity. Under the experimental conditions above, only a small fraction of the pump pulse is required to achieve this complete absorption saturation.

The pump pulse is long compared with the time taken for an effective carrier temperature to be established, and our numerical modeling[10] of the net energy-loss rate of the excess carrier energy to the lattice via deformation-potential scattering indicates that over the range of electron concentrations used throughout this study, the carrier temperatures approach the lattice temperature to within 2% in less than 3 ps. The total pump energy absorbed by the sample during each pump pulse would result in a peak temperature increase of the InAs of only
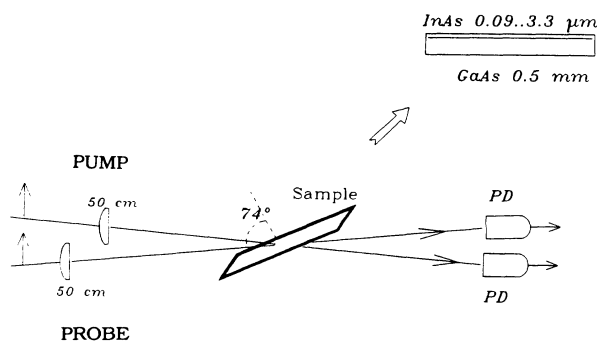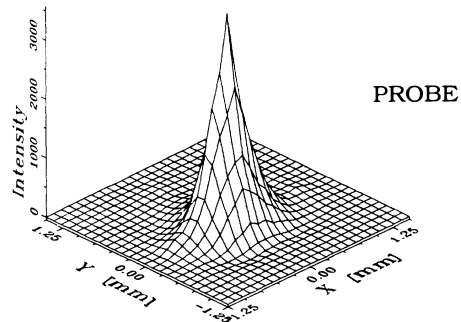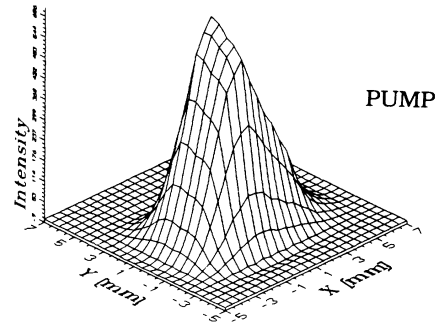

FIG. 2. Experimentally measured intensity profiles (in arbitrary units) of the pump and probe beams in the plane perpendicular to the propagation direction.

0.02 K per pulse, and we hence neglect lattice-heating effects.

The net effect of the above is that the initial carrier distribution in the InAs epilayers just after excitation has an effective temperature equal to the 300-K lattice and is independent of fluctuations in the pump-pulse intensity. The total carrier concentration, however, scales as $(h\nu_{pu} - E_g)^{1/2}$. When the subsequent recovery of sample absorption is measured at a fixed wavelength (generally equal to the pump wavelength), nonexponential absorption transients are expected, but bleaching recovery occurs on a time scale of the order of the mean carrier recombination time.

III. EXPERIMENTAL RESULTS

Figure 3 shows the result of a spectrally resolved experiment where the pump-pulse wavelength and the time delay between the pump and probe beams are fixed, while the wavelength of the probe pulse is changed. Curve 1 [Fig. 3(a)] is the small-signal absorption spectrum $A_0(h\nu)$ of 3.3-μm-thick InAs ($A(h\nu) = -\ln[T(h\nu)]$, where T is the sample transmission); curve 2 is a dynamic spectrum

FIG. 1. Experimental setup for the pump-probe-spectroscopy experiments. PD-PbSe infrared photodetectors.

TABLE I. InAs parameters at 300 K (Ref. 5).

E_g (eV)	E_{so} (eV)	m_e/m_0	m_{hh}/m_0	m_{lh}/m_0
0.35 (2825 cm^{-1})	0.37 (2885 cm^{-1})	0.022	0.4	0.026

$A(h\nu)$ taken 20 ps after excitation at $h\nu = 446$ meV. One can see a dramatic change in the absorption spectrum due to the band-filling effect. The large difference in the electron and hole effective masses (see Table I) gives a 77-fold density-of-states ratio between the valence and conduction bands and the observed DMS is dominated by shifts in the electron quasi-Fermi level.

The electron-occupation probability $f_e(E - E_c)$ [Fig. 3(b)] corresponding to curve 2 in Fig. 3(a) is calculated from the measured dynamic spectrum using the relation[11]

$$A(h\nu) = A_0(h\nu)\frac{1 - f_e(E_e^{\mathrm{hh}}) - f_{\mathrm{hh}}(E_{\mathrm{hh}}^{\mathrm{hh}}) + \kappa[1 - f_e(E_e^{\mathrm{lh}}) - f_{\mathrm{lh}}(E_{\mathrm{lh}}^{\mathrm{lh}})]}{1 + \kappa} \; ,$$ (1)

where $f_e(E_e)$, $f_{\mathrm{hh}}(E_{\mathrm{hh}})$, and $f_{\mathrm{lh}}(E_{\mathrm{lh}})$ are the electron, heavy-hole, and light-hole occupation probabilities respectively, and the hh and lh superscripts denote the energies of the carriers in those bands that participate in the e-hh and e-lh transitions, respectively. Here, the joint density-of-states factor

$$\kappa = (\mu_{\mathrm{lh}}/\mu_{\mathrm{hh}})^{3/2} = 0.43 \; ,$$

where

(a)

(b)

FIG. 3. (a) InAs $(d = 3.3 \; \mu\mathrm{m})$ absorption: 1, without excitation; 2, 20 ps after excitation at $h\nu_{\mathrm{pump}} = 3600 \; \mathrm{cm}^{-1}$. (b) Experimental electron-occupation probability function corresponding to curve 2 [(a)]; solid line represents the Fermi distribution with E_F equal to 110 meV above the conduction-band minimum and an electron temperature of 300 K.

$$\mu_{\mathrm{lh}} = m_e m_{\mathrm{lh}}/(m_e + m_{\mathrm{lh}})$$

and $\mu_{\mathrm{hh}} = m_e m_{\mathrm{hh}}/(m_e + m_{\mathrm{hh}})$, using the InAs parameters listed in Table I.

We use a parabolic three-band model of InAs to describe the absorption as transitions from the splitoff band (≈ 0.37 eV below the valence band) are outside the spectral range of interest here. We also neglect band-gap-renormalization (BGR) effects, because we believe them to be negligible compared with the DMS absorption-edge shift due to the small InAs electron mass. According to Ref. 2, BGR lowers the band edge by ≈ 0.3 meV in InAs at electron concentrations $n_e = 1.5 \times 10^{16}$ cm^{-3} and, assuming a $n_e^{1/3}$ carrier-density dependence of the BGR shift, we estimate a maximum BGR of only 1.1 meV at $n_e = 8 \times 10^{17}$ cm^{-3}, the highest nonequilibrium electron concentration used in our experiment. This compares with a band-filling shift of ≈ 110-meV change in the electron quasi-Fermi level at this concentration.

Electron-occupation functions $f_e(E - E_c)$ were numerically extracted from the induced absorption spectra using relation (1) in conjunction with the knowledge that at all times the electron and hole concentrations are equal. A typical example is shown in Fig. 3(b) [derived from the induced absorption spectrum 3(a)] and it closely follows a Fermi function with a quasi-Fermi energy of 110 meV above the bottom of the conduction band and an electron temperature of 300 K. Also apparent [Fig. 3(a), curve 2] is a negative absorption (amplification) region extending from 3200 cm^{-1} to the band edge at ≈ 2820 cm^{-1}, due to population inversion from the high electron concentrations rapidly thermalizing towards the conduction-band minimum.

Total nonequilibrium carrier concentrations as a function of delay after excitation were calculated with a high accuracy ($\pm 5\%$) by integrating the measured f_e distributions. In the case of Fig. 3, $n_e = 6 \times 10^{17}$ cm^{-3}.

Figure 4 shows the pump-density dependence (at $h\nu_{\mathrm{pump}} = 3600$ cm^{-1}) of the transmission of the 3.3-μm-thick InAs sample at the same wavelength. The induced transmission is measured with a 20-ps delay between pump and probe pulses, i.e., the delay where the bleaching effect reaches its maximum, and the peak transmission is seen to reach unity at pump densities about an order of magnitude lower than were used in the time-resolved-spectroscopy experiments. Figure 4 is in excellent agreement with the simple band-filling model and calculations show that the charge carriers are created with a quantum efficiency close to unity.
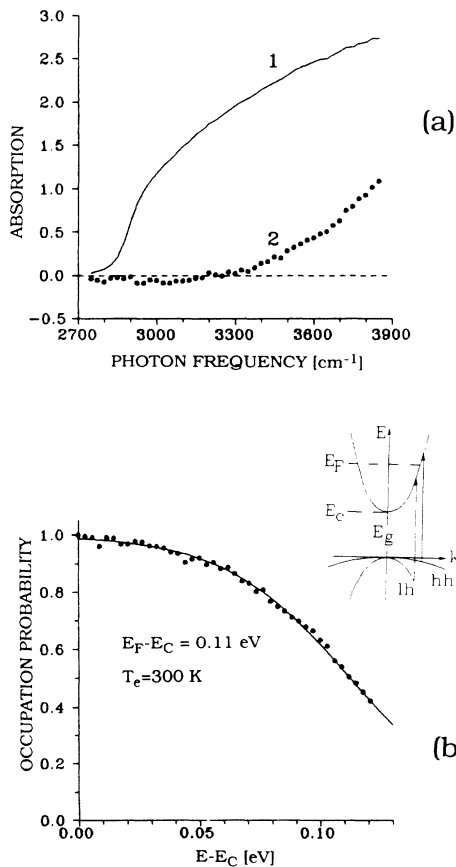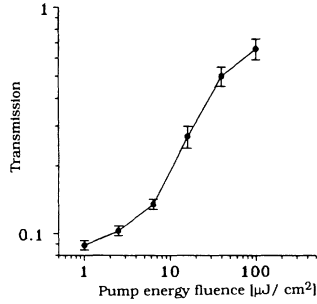
FIG. 4. InAs ($d = 3.3$ μm) transmission at $h\nu_{probe} = 3600$ cm^{-1} vs pump fluence at the same wavelength, measured at a pump-probe delay $\tau_{del} = 20$ ps.

In time-resolved experiments (Fig. 5), the light frequencies $h\nu_{pump} = h\nu_{probe} = h\nu$ were held fixed while the time delay between the pulses was varied. Figure 5(a) shows the observed strong dependence of the absorption recovery time as a function of the photon energy, characterized here by $\tau_{1/2}$, the time taken for the optical-density change to decrease by a factor of 2. For example, we find $\tau_{1/2} \approx 3000$ ps at $h\nu = 3000$ cm^{-1}/371 meV compared

with $\tau_{1/2} \approx 250$ ps at $h\nu = 3800$ cm^{-1}/471 meV. As shown in Fig. 5(b), the bleaching dynamics are also very sensitive to the thickness of the InAs layer. At pump-probe photon frequencies of 3600 cm^{-1}, $\tau_{1/2}$ changes from 450 ps in the 3.3-μm-thick layer to 35 ps in the 0.09-μm sample.

Some of the samples studied were irradiated with high-energy protons to produce controlled point-defect concentrations in the InAs and corresponding artificially decreased recovery times [Fig. 5(c)]. The proton energies were chosen (using the "TRIM" Monte Carlo ion-implantation modeling program[12]) so that the peak in the implanted defect-density profile lay in the center of the InAs layer in each case. For the 3.3-, 0.6-, and 0.27-μm-thick samples, the proton energies were 200, 45, and 15 keV, respectively. For the 3.3-μm-thick InAs sample irradiated at a proton dose of 10^{14} cm^{-2}, $\tau_{1/2}$ decreased to ≈ 130 ps at $h\nu = 3600$ cm^{-1}/446 meV, compared with $\tau_{1/2} \approx 450$ ps for the as-grown sample at the same wavelength. A similar, although less controllable, reduction in $\tau_{1/2}$ (from 200 to 80 ps) was also achieved by mechanical lapping of the 0.6-μm sample from the InAs side with 0.25-μm diamond paste [Fig. 5(d)].
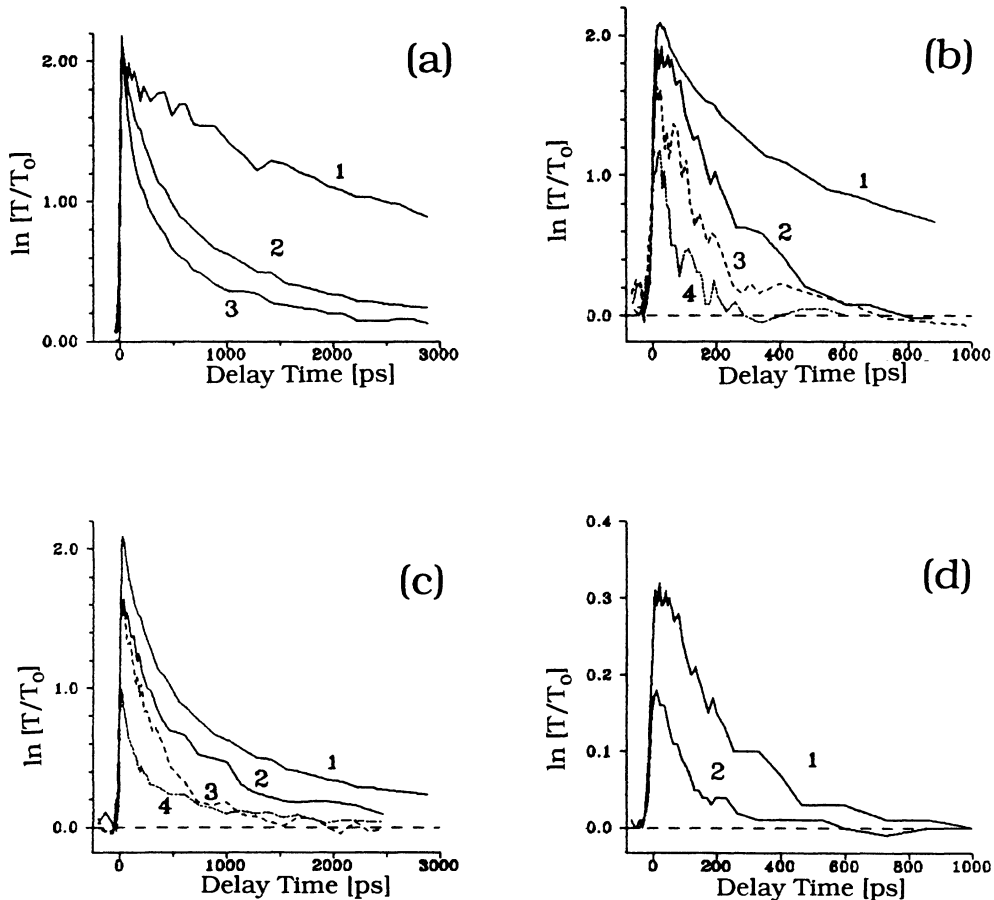

FIG. 5. Transmission change as a function of pump-probe delay for $h\nu_{pump} = h\nu_{probe} = h\nu$: (a) 1, $h\nu = 3000$ cm^{-1}; 2, $h\nu = 3600$ cm^{-1}; 3, $h\nu = 3800$ cm^{-1} ($d = 3.3$ μm); (b) $h\nu = 3600$ cm^{-1}, 1, $d = 3.3$ μm; 2, $d = 0.6$ μm; 3, $d = 0.18$ μm; 4, $d = 0.09$ μm; (c) $d = 3.3$ μm; $h\nu = 3600$ cm^{-1}; 1, as-grown sample; 2, 10^{12} cm^{-2} proton dose; 3, 10^{13} cm^{-2} proton dose; 4, 10^{14} cm^{-2} proton dose; (d) $d = 0.6$ μm; 1, as-grown sample; 2, after diamond lapping.

IV. DISCUSSION

The calculated radiative lifetime for an electron recombining with a hole in InAs is 2.8 ns (Ref. 4) based on the known interband dipole matrix element. This value, however, only applies to all the carriers if they are in completely degenerate distributions. In nondegenerate conditions, each electron makes transitions to states where the mean hole-occupation factor $f_{hh(lh)}$ is less than unity. In our experimental regime, the hole-occupation probability near the top of the valence band never exceeds 0.1 at the maximum carrier densities achieved, giving calculated radiative recombination times in these samples that are always ≥ 25 ns. This is ≈ 40 times larger than the longest $\tau_{1/2}$ values measured and we thus consider the role of radiative recombination processes to be negligible here.

The bleaching-recovery-time $\tau_{1/2}$ dependencies on the pump light frequency, InAs thickness, and proton bombardment dose are shown in Fig. 6. The behavior of the curves in Figs. 6(b) and 6(c) can be qualitatively explained in terms of the influence of lattice defects in decreasing the carrier lifetime.

The 7% lattice-constant mismatch between InAs and GaAs produces a large misfit dislocation density (of the order of 10^{10} cm^{-2}) at the growth interface between the two semiconductors. These dislocations significantly enhance the carrier recombination rates. It is clear that the comparative importance of the interface defects between InAs and GaAs is larger when the InAs thickness is smaller, accounting for the results of Fig. 6(b), and a surface recombination velocity model[13] gives good quantitative agreement for the dependency of lifetime on layer thickness if a sample independent-interface-recombination velocity of $2.7\pm0.3\times10^4$ cm s^{-1} is assumed.

Proton bombardment creates additional Shockley-Read volume defects, thereby decreasing the carrier lifetime [Fig. 6(c)]. The apparent increase of the decay time for the 3.3- and 0.6-μm-thick samples for proton doses $>10^{14}$ cm^{-2} is probably an artifact due to the breakdown of the simple parabolic band and of the intrinsic equilibrium carrier concentration assumptions and will be discussed in detail elsewhere.[13]

Figure 7(a) shows the dependence of the electron decay rate $\tau^{-1}=(1/n_e)dn_e/dt$ as a function of n_e, where τ is the effective carrier recombination time. For $n_e < 2 \times 10^{17}$ cm^{-3}, the decay rate varies widely depending on sample thickness and is generally dominated by the nonradiative recombination at the InAs-GaAs interface defects and Shockley-Read recombination at volume defects.

For $n_e > 2\times10^{17}$ cm^{-3}, however, there is a strong and systematic variation in the effective recombination time with carrier concentration that follows a $\tau^{-1}=An_e^2$ law with increasing accuracy as n_e increases. This n_e dependence is characteristic of an Auger recombination process and the coefficient A, derived from a straight-line fit to the data [Fig. 7(a)], is $(1.1\pm0.1)\times10^{-26}$ cm^6 s^{-1}.

The experimental data for a wide range of pump-light wavelengths with the 3.3-μm-thick sample all fit the same straight line in Fig. 7(a) and the experimental data for the

thinner samples (not shown), although of poorer quality due to the increased importance of the additional extrinsic recombination channels, are also fully consistent with this value of the Auger coefficient.

Thus, the behavior of the plot in Fig. 6(a) can be understood qualitatively in terms of the Auger effect. As the pump photon energy is increased, the carrier concentration at the onset of the absorption transient also increases as $n_e \sim (h\nu - E_g)^{3/2}$, and the n_e^2 dependence of the Auger
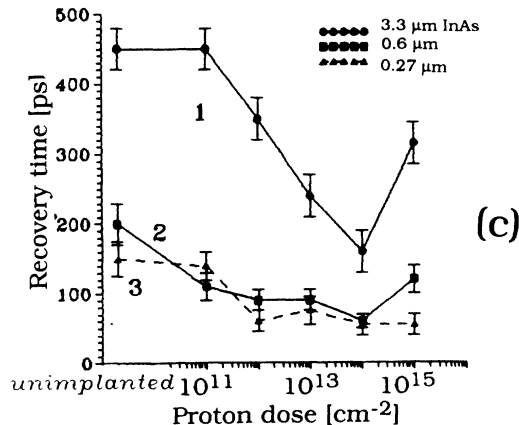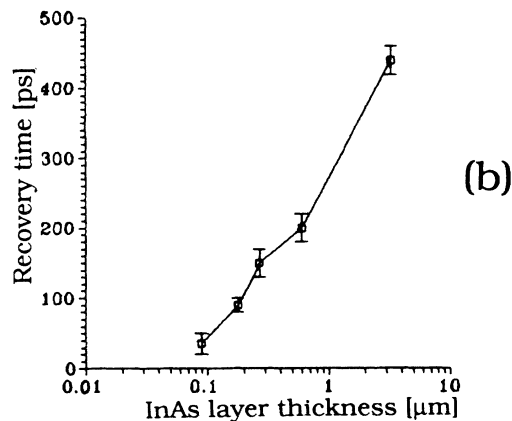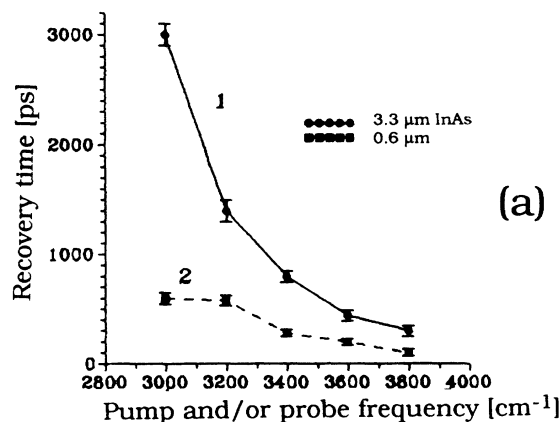

FIG. 6. Bleaching recovery-time $\tau_{1/2}$ dependence on (a) pump-probe photon energy; (b) InAs layer thickness; (c) proton dose.

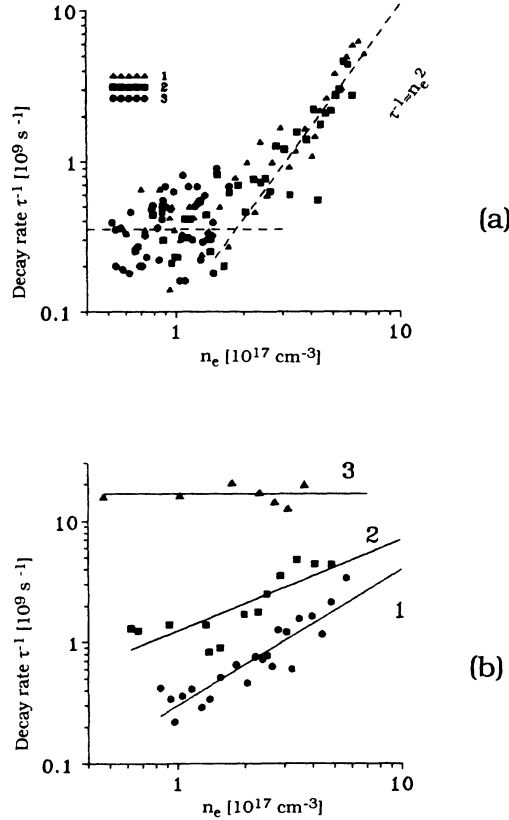FIG. 7. Effective carrier lifetime as a function of nonequilibrium electron density: (a) $d = 3.3$ μm; 1, $h\nu = 3800$ cm^{-1}; 2, $h\nu = 3600$ cm^{-1}; 3, $h\nu = 3000$ cm^{-1}; (d) 1, $d = 3.3$ μm as-grown, $h\nu = 3600$ cm^{-1}; 2, $d = 3.3$ μm $\times 10^{14}$ cm^{-2} proton bombarded, $h\nu = 3600$ cm^{-1}; 3, $d = 0.09$ μm as-grown, $h\nu = 3600$ cm^{-1}.

recombination rate means that recombination is strongly accelerated at high n_e and the mean carrier lifetime and, hence, the apparent bleaching recovery time decreases with increasing pump photon energy.

For the case $m_e^* \ll m_h^*$ and for unscreened Auger scattering processes between nondegenerate carriers in parabolic bands in thermal equilibrium, Ridley[14] derives the following approximate expression for the total Auger scattering rate per electron:

$$W_{eq} = \frac{2\pi^{1/2}e^4 m_e^* (kT)^{3/2}[(m_e^*/m_0)+M]}{(\varepsilon_0\varepsilon_r)^2 \hbar^3 (1+M)^{1/2}E_g^{3/2}}$$

$$\times \exp[-(1+M)E_g/(kT)] , \qquad (2)$$

where $M = m_e^*/m_h^*$ and ε_r, the InAs dielectric constant, is taken as 15.15.[5] In the presence of nonequilibrium electron and hole carrier concentrations n and p, this expression is modified to

$$W_{n\text{-}eq} = W_{eq}(np/n_i^2) .$$

As W is simply the inverse of the electron lifetime τ, the above expression can be used to calculate an expected value of the Auger coefficient A through $A = W_{eq}/n_i^2$,

and using the values tabulated above gives a value of $A = 1.23 \times 10^{26}$ cm^6 s^{-1}. The derivation of the expression for W_{eq} involves a number of approximations and at the n_e values at which we were able to measure A, the electron quasi-Fermi level is $\approx 2kT$, and the assumption of nondegenerate carrier statistics is questionable. Nevertheless, the close coincidence between the measured and calculated values is impressive, although at least in part fortuitous, and gives us additional confidence in our identification of the physical mechanism dominating the recombination in these samples for $n_e \geq 2 \times 10^{17}$ cm^{-3}.

In Fig. 7(b) the decay rate versus electron-density dependencies are compared for the cases of (1) 3.3-μm-thick as-grown, (2) 3.3-μm-thick proton-irradiated at 10^{14} cm^{-2}, and (3) 0.09-μm unimplanted samples. In case (2), a weak Auger effect is still apparent, even though the heavy proton dose has substantially increased the decay rate at low n_e. In the case of the very thin sample (3), the effect of recombination at the InAs/GaAs interface dominates and the effective lifetime is independent of n_e. Generally, under the present experimental conditions ($n_e = 10^{16} - 8 \times 10^{17}$ cm^{-3}), defect recombination at the InAs/GaAs interface starts to dominate over the Auger effect for InAs epilayer thicknesses less than 0.5 μm.

V. CONCLUSION

Picosecond pump-probe experiments have been performed close to and above the band edge in undoped InAs MBE samples. At excitation intensities of $1-2 \times 10^7$ W cm^{-2}, large dynamic Moss-Burstein shifts up to 80–90 meV (700 cm^{-1}) were found corresponding to excess carrier concentrations of 8×10^{17} cm^{-3} and leading to pronounced absorption bleaching near the excitation wavelength with a recovery time that varied in the range of 3000–35 ps and was strongly dependent on the excitation wavelength, sample thickness, and proton implantation dose. The measured Auger coefficient is in excellent agreement with the calculations of Ridley, and is found to dominate the recombination dynamics for InAs epilayer thicknesses greater than ≈ 0.5 μm.

Analysis of the thickness dependence of the bleaching recovery time shows that the latter can be further decreased (probably down to ≈ 1 ps) by decreasing the InAs layer thickness. This result is important for laser intracavity saturable absorber applications, where the required optical density can be achieved in MBE epilayers by growing an appropriate number of InAs layers sandwiched between transparent GaAs cladding layers. Such heterostructures should be effective in obtaining the shortest possible ir ps pulses when used as passive mode-locking elements.

[1]C. D. Poole and E. Garmire, Appl. Phys. Lett. **44**, 363 (1984).

[2]C. D. Poole and E. Garmire, IEEE J. Quantum Electron **QE-21**, 1370 (1985).

[3]V. I. Kovalev, M. B. Suvorov, and V. A. Trofimov, Infrared Phys. **31**, 343 (1991).

[4]C. C. Phillips, Y. B. Li, R. A. Stradling, and K. L. Vodopyanov, J. Phys. D **24**, 437 (1991).

[5]Author, in *Numerical Data and Functional Relationships in Science and Technology,* edited by editor Landolt-Börnstein, New Series Group III, Vol. 22a (Springer, Berlin, 1987), pp. 117–118.

[6]K. L. Vodopyanov, A. V. Lukashev, C. C. Phillips, and I. T. Ferguson, Appl. Phys. Lett. **59**, 1658 (1991).

[7]P. D. Wang, S. N. Holmes, Tan Le, R. A. Stradling, I. T. Ferguson, and A. G. de Olivera, Semicond. Sci. Technol. 7, (1992).

[8]Y. B. Li and R. A. Stradling (private communication).

[9]H. Graener, R. Dohlus, and A. Laubereau, Chem. Phys. Lett. **140**, 306 (1987).

[10]Carrier energy-loss rates were computed by integrating the expressions in Sec. 3.5 of Ref. 14 over the experimentally measured carrier distributions.

[11]P. Lavallard, R. Bichard, and C. Benoit a la Guillaume, Phys. Rev. B **16**, 2804 (1977).

[12]J. F. Zeigler, *Ion Implantation Science and Technology,* 2nd ed. (Academic, New York, 1988), pp. 1–61.

[13]K. L. Vodopyanov, H. Graener, C. C. Phillips, I. T. Ferguson, and T. Tate (unpublished).

[14]B. K. Ridley, *Quantum Processes in Semiconductors* (Clarendon, Oxford, 1988), pp. 269–276.